International Journal of Minerals, Metallurgy and Materials
Volume 24, Number 3, March 2017, Page 309
DOI: 10.1007/s12613-017-1409-2

Microstructure and properties of mullite-based porous ceramics produced from coal fly ash with added Al_2O_3

Jian-bin Zhu[1,2] *and Hong Yan*[1]

1) Department of Materials Processing Engineering, School of Mechanical Electrical Engineering, Nanchang University, Nanchang 330000, China
2) School of Mechanical Electrical Engineering, Nanchang Institute of Technology, Nanchang 330000, China
(Received: 11 July 2016; revised: 1 November 2016; accepted: 2 November 2016)

Abstract: Using coal fly ash slurry samples supplemented with different amounts of Al_2O_3, we fabricated mullite-based porous ceramics via a dipping-polymer-replica approach, which is a popular method suitable for industrial application. The microstructure, phase composition, and compressive strength of the sintered samples were investigated. Mullite was identified in all of the prepared materials by X-ray diffraction analysis. The microstructure and compressive strength were strongly influenced by the content of Al_2O_3. As the Al/Si mole ratio in the starting materials was increased from 0.84 to 2.40, the amount of amorphous phases in the sintered microstructure decreased and the compressive strength of the sintered samples increased. A further increase in the Al_2O_3 content resulted in a decrease in the compressive strength of the sintered samples. The mullite-based porous ceramic with an Al/Si molar ratio of 2.40 exhibited the highest compressive strength and the greatest shrinkage among the investigated samples prepared using coal fly ash as the main starting material.

Keywords: porous materials; ceramics; fly ash; mullite; aluminum oxide

1. Introduction

Because of their low thermal expansion coefficient, high permeability, good chemical stability, and excellent mechanical properties at elevated temperature, porous mullite ceramics are considered good candidate materials for gas/liquid filters [1], catalyst supports [2], separation membranes [3], and membrane supports [4–8]. Porous mullite ceramics have been fabricated from various starting materials, including mullite powder [1–2,9], kyanite [10], bauxite [11–12], kaolin [13], coal gangue [12], and coal fly ash [3,5–9,11,14–17]. These materials contain abundant SiO_2 and Al_2O_3 and can be categorized as fine chemicals, minerals, or wastes. Among these, wastes are regarded as the most meaningful starting materials from the viewpoint of resource conservation and cost reduction. In particular, coal fly ash, an abundantly available industrial waste generated during the combustion of raw coal in thermal power plants and which can cause soil, water, and air pollution and other environmental problems if not properly treated [18], has attracted much attention recently as a starting material for porous mullite ceramics. Because this process enables the efficient recycling of waste fly ash, it not only decreases environmental pollution but also results in high-value-added products.

Several processing methods have been developed to fabricate porous mullite ceramics, including the casting and reaction sintering method [10]. Porous ceramics prepared directly by this method often exhibit good mechanical strength but poor open porosity. Additives are therefore used to create a more highly porous structure while maintaining a high mechanical strength at lower sintering temperatures. Additive combinations of bauxite and WO_3 [3], AlF_3 and $Al(OH)_3$ [4], bauxite and titania [5], AlF_3 and MoO_3 [7], and AlF_3 and V_2O_5 [11] have been confirmed to achieve these effects when coal fly ash is the main starting material of porous mullite ceramics. However, ceramics with greater than 60% open porosity are difficult to obtain by this method. Other methods, such as foam-gelcasting [1–2], freeze

Corresponding author: Hong Yan E-mail: hyan@ncu.edu.cn

casting [15–16], and the replica method [19], have therefore been developed to prepare high-open-porosity porous mullite ceramics. Among these methods, the replica method is the most common route for producing reticulated porous ceramics and has been well exploited in industry. The replica method is based on the impregnation of a polymer sponge with a ceramic suspension or precursor solution to produce a macroporous ceramic that exhibits the same morphology as the original porous material. The pore size distribution and open porosity—two of the most important parameters governing the permeability of porous ceramics—can be well controlled by the replica method; thus, the replica method is one of the most attractive options for the rapid development of an industrial approach suitable for recycling coal fly ash to manufacture porous mullite ceramics with a well-controlled pore morphology.

An SiO_2 amorphous glass phase is abundant in coal fly ash; this phase adversely affects the mechanical properties and alkali corrosion resistance of the resulting ceramic products and limits their application range. Approaches to reduce the amount of the amorphous glass phase in the ceramic products and thereby improve their mechanical and corrosion resistance properties are therefore a topic of great interest. Al_2O_3 can react with the SiO_2 glass phase and form mullite, which has excellent mechanical and corrosion resistance properties. In previous works, bauxite [3,5,11], $Al(OH)_3$ [4,14], AlF_3 [4,7,11], pure Al_2O_3 [15–16], and some other Al_2O_3 sources have been added to coal fly ash to prepare starting material mixtures with an Al/Si molar ratio of 3.00 for the subsequent fabrication of porous mullite. However, a molar ratio of 3.00 may not be appropriate for the raw materials of porous ceramics derived from coal fly ash because coal fly ash contains other metal oxides (e.g., Fe_2O_3) that react with the SiO_2 glass phase to form a low-melting-point material. The resulting deficiency of SiO_2 would lead to crystallization of Fe_2O_3, which can decrease both the mechanical and acid corrosion resistance properties of the porous ceramics. Thus, the Al_2O_3 content likely strongly influences the properties of porous ceramics produced from coal fly ash.

The present work was aimed at studying the effects of Al_2O_3 on the microstructure and properties of porous ceramics produced from coal fly ash and developing an effective approach to fabricating macroporous ceramics suitable for industrial application. Therefore, porous ceramics were prepared using coal fly ash slurry samples with different contents of Al_2O_3 by a dipping-polymer-replica approach. The microstructure, phase compositions, and properties of the products were investigated.

2. Experimental

2.1. Raw materials

As the main starting material, coal fly ash from the Nanchang Thermal Power Plant in Jiangxi Province, China, was used. As shown in Fig. 1(a), the fly ash consists of particles with sizes less than 500 μm. The morphological details of the surface of the fly ash are shown in Fig. 1(b). X-ray diffraction (XRD) analysis revealed the major crystalline phases of the fly ash to be mullite, quartz, and other metasilicates (Fig. 2). The chemical composition of the fly ash is listed in Table 1.

In addition, Al_2O_3 (Tianjin Yongda Chemical Reagent Co. Ltd., China), starch (Taishan Chemical Factory Co. Ltd., China), and polyurethane sponge (Dongguan Donghong Sponge Products Factory, China) were used as an additive, a curing agent, and a polymer template, respectively.

The burn-out stage of the starch and polyurethane sponge was carried out carefully using a suitable heating rate and an appropriate temperature to avoid destruction of the porous ceramic structure [19]. The thermal behaviors of the starch and polyurethane sponge were therefore determined by thermogravimetry/differential thermal analysis (TG/DTA) in air using a heating rate of 10°C/min. As shown in Fig. 3(a), the

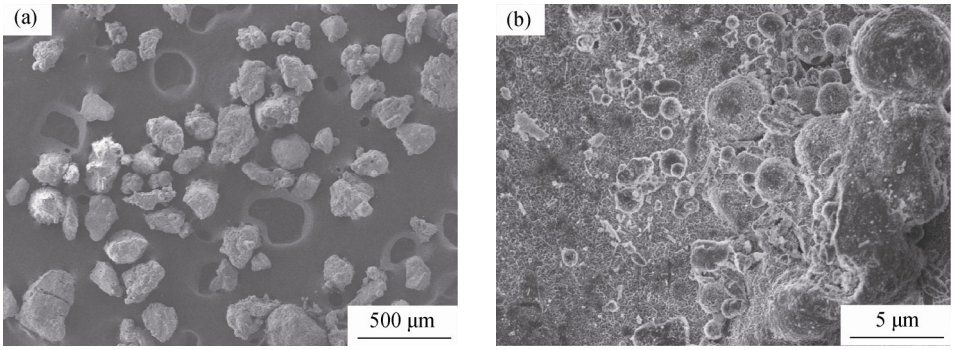

Fig. 1. Scanning electron micrographs showing the morphology of the coal fly ash.

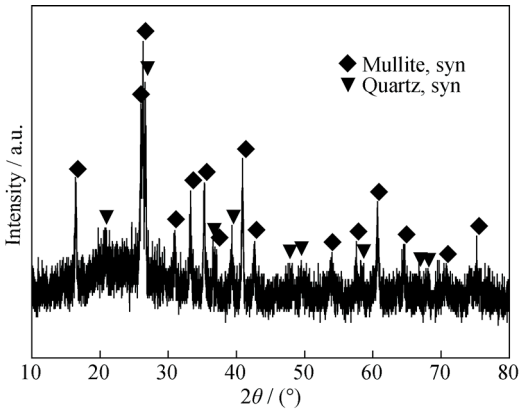

Fig. 2. XRD pattern of the coal fly ash.

mass loss of starch occurred in three stages: moisture evaporation (70–150°C), thermal decomposition (250–400°C), and remainder oxidation (400–550°C). No significant mass loss occurred at temperatures greater than 550°C. The thermal decomposition of polyurethane sponge occurred mainly in the range from 220 to 550°C, as shown in Fig. 3(b). Notably, the burn-out stage of the starch and polyurethane sponge was almost completed at temperatures below 550°C. The burn-out stage is very important for preventing destruction of the ceramic structure by the high pressures of the generated gas. Therefore, a slow heating rate to 550°C should be used in the sintering process.

Table 1. Composition of the coal fly ash, as detected by X-ray fluorescence wt%

SiO_2	Al_2O_3	Fe_2O_3	CaO	TiO_2	K_2O	SO_3	Na_2O	MgO	SrO	Others
50.70	36.38	5.63	3.59	1.36	0.49	0.46	0.33	0.23	0.19	0.64

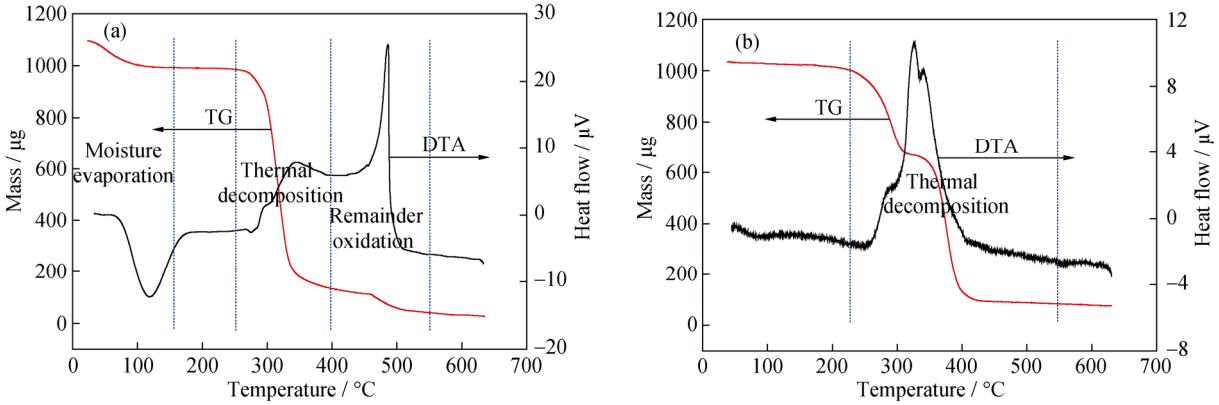

Fig. 3. TG/DTA curves for (a) starch and (b) polyurethane in air.

2.2. Processing

The raw materials in certain ratios (Table 2) calculated on the basis of the X-ray fluorescence (XRF) analysis results were mixed and ball-milled for 12 h to obtain aqueous slurry samples with a solid loading of 65wt%. Cylinder polyurethane sponges with 30 pores per inch (PPI), 64 mm in diameter, and 20 mm high, were immersed in the slurry, compressed repeatedly to fill all the pores, and then removed from the slurry. After being squeezed to remove the excess slurry, the green bodies were dried at 80°C for 12 h. On the basis of the TG/DTA analysis results in Fig. 3, the dried green bodies were sintered using the following two-step procedure: (1) heating to 550°C for 1 h at a rate of 2°C/min to burn out the starch and the sponges, followed by (2) heating to 1600°C [20] for 4 h at a rate of 10°C/min to sinter the ceramics and then cooling to room temperature.

Table 2. Compositions of the starting material samples

Sample	Fly ash / wt%	Al_2O_3 / wt%	Starch / wt%	Al/Si mole ratio
S1	95.00	0	5	0.84
S2	71.66	23.34	5	1.60
S3	56.87	38.12	5	2.40
S4	49.24	45.76	5	3.00

2.3. Characterization

The macromorphology, porosity, skeleton density, linear shrinkage, compressive strength, dominant phase, microstructure, and energy-dispersive X-ray spectrum (EDS) of the prepared porous ceramics were investigated. The macromorphology was captured using a normal camera. The skeleton volume and the porosity were measured by the Archimedes displacement method using water as a medium.

The skeleton density was obtained from the ratio of the sample mass to the skeleton volume. The linear shrinkage of samples during sintering was determined using the following equation:

$$s = \frac{l_g - l_s}{l_g} \times 100\%,$$

where s is the linear shrinkage of samples, l_g is the length of green samples, and l_s is the length of sintered samples. The results of the porosity, skeleton density, and linear shrinkage of the samples are presented as the mean values of five measurements.

The dominant phases in the sintered samples were identified by XRD (Bruker D-8). The normalized reference intensity ratio (RIR) method [21–23] was employed to semi-quantify the phase contents of the sintered ceramic products.

The microstructure was observed and EDS was performed by SEM (JEOL, JSM-6701F). The compressive strength was measured using a testing machine (MTS YAW6206), and all of the compressive strength results are presented as the mean values of fifteen measurements.

3. Results and discussion

3.1. Crystalline phases and microstructures

The XRD patterns of the sintered samples are shown in Fig. 4. Quartz (SiO_2, syn PDF#46-1045) was identified in samples S1 and S2, and less was observed in samples S3 and S4. The peaks of hematite (Fe_2O_3, syn PDF#33-0664), which can adversely affect both the mechanical and acid corrosion resistance properties of the porous ceramics, were weak in the pattern of S3 and more intense in the pattern of S4. Trace corundum (Al_2O_3, syn PDF#46-1212) was also identified in sample S4. The dominant phase in all of the samples was mullite ($3Al_2O_3{\cdot}2SiO_2$, syn PDF#15-0776).

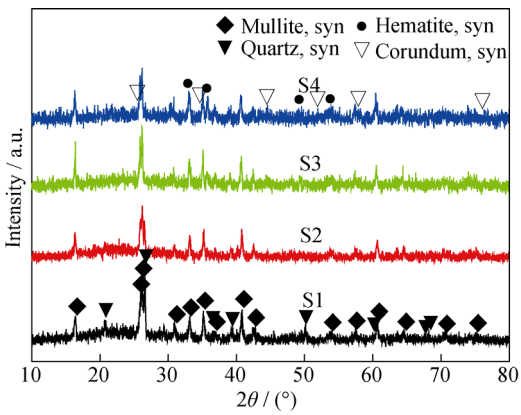

Fig. 4. XRD patterns of the porous ceramic samples.

According to the calculation results obtained by the RIR method, the phase contents of mullite in samples S1, S2, S3, and S4 were 56.1wt%, 69.3wt%, 81.8wt%, and 87.6wt%, respectively. Thus, increasing Al_2O_3 content promoted mullitization of the ceramics. All four samples are regarded as mullite-based porous ceramic composites.

The microstructures of the porous ceramic skeletons are shown in Fig. 5. All four samples have skeletons with crossed banded structures. The composition of the banded structure in S3 is shown in Fig. 6. The amorphous phase was observed in samples S1, S2, and S3. With increasing Al_2O_3 content, the amount of the amorphous phase decreased and the banded structures developed increasingly distinct boundaries. In addition, the sizes of banded structures in all four samples differed. Sample S1 (Fig. 5(a)) exhibited the largest banded structures among the investigated samples.

The effects of Al_2O_3 on the XRD patterns and the microstructures of porous ceramic skeletons were mediated by changing the Al/Si molar ratio of the starting materials, which can determine the reactions that occur during the sintering process.

$$SiO_2(\text{amorphous}) + \text{Metasilicate} = SiO_2(\text{crystal}) + \text{AP}(\text{amorphous } SiO_2 + \text{metasilicate}) \quad (1)$$

$$2SiO_2(\text{amorphous or crystal}) + 3Al_2O_3 = 3Al_2O_3 \cdot 2SiO_2 \quad (2)$$

In the case of sample S1, which contained no added Al_2O_3, the reaction in Eq. (1) occurred during the sintering process. The amount of crystalline quartz identified by XRD (the curve for sample S1 in Fig. 4) is greater than that in the original coal fly ash (Fig. 2). The amorphous phase, as shown in Fig. 5(a), contains excess SiO_2 and metasilicate. The abundant amorphous phase, which is a low-viscosity liquid at the high sintering temperature, promotes the formation of large banded structures [14], which explains why the banded structures in Fig. 5(a) are the largest among the investigated samples.

In the case of samples with added Al_2O_3, the reactions in Eqs. (1) and (2) occurred during the sintering process. The reaction in Eq. (2) increases the mullite content and decreases the amorphous phase. Accordingly, the viscosity of the sintering system increased and the banded structures were smaller than those in sample S1. However, because sample S2 lacked Al_2O_3, its banded structures were approximately the same size as those in sample S3, although sample S2 had lower viscosity liquid in the sintering process than sample S3. Conversely, because sample S4 contained abundant Al_2O_3, it contained little SiO_2 to form the amorphous phase, resulting in the smallest banded structures among the investigated samples.

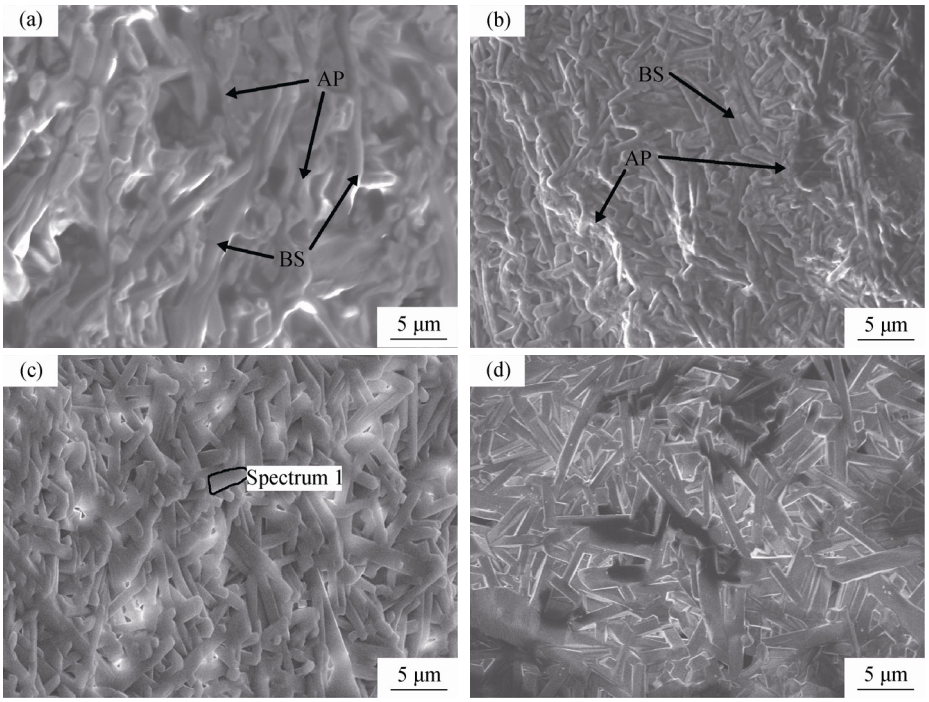

Fig. 5. Microstructures of the porous ceramic skeletons: (a) S1; (b) S2; (c) S3; (d) S4 (AP: amorphous phase; BS: banded structure).

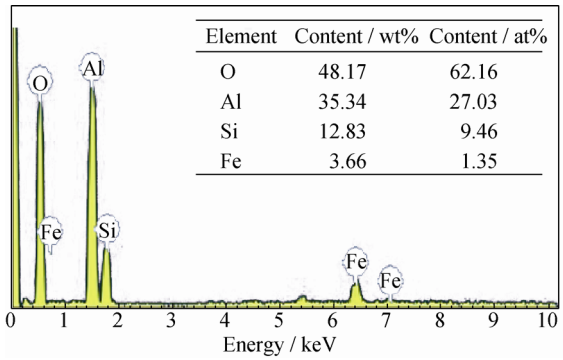

Fig. 6. EDS spectrum of the banded structure in Fig. 5(c).

Trace corundum and quartz were identified in the S3 and S4 sintered materials because of the presence of alkaline metallic oxide, which can cause decomposition of the mullite at high temperatures, especially in a system with a high degree of mullitization. Moreover, mullite can accommodate transitional-metal cations [24]. As shown in Fig. 6, Fe was accommodated into mullite banded structures. With increasing Al_2O_3 content, Fe was released from the mullite system and formed hematite (Fe_2O_3), which was identified in the XRD patterns (curves for samples S3 and S4 in Fig. 4).

3.2. Morphology and properties

As shown in Fig. 7, the sintered samples exhibited different colors and similar optical macromorphologies. Sample S1 exhibited a thick dark color, whereas sample S4 exhibit a light-brown color. The color of the samples changed with increasing Al_2O_3 content and was mainly determined by the reaction products. The amorphous phase, which contained excess amorphous SiO_2 and metasilicate, imparted samples S1 and S2 with dark colors. The reddish-brown hematite imparted samples S3 and S4 with a brown color. All of the samples had interconnected skeletons and open pores like those of the template sponges except for the size shrinkage.

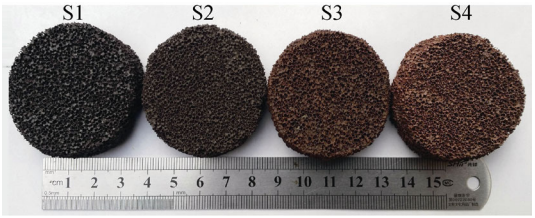

Fig. 7. Optical macromorphology of the samples.

More morphological details were obtained from SEM micrographs, as shown in Fig. 8. Samples S1 and S2 exhibited some small cracks in the ceramic matrix, and more cracks were observed in sample S4, whereas almost none were observed in sample S3. Sample S3 also exhibited the lowest porosity and the highest skeleton density, as shown in Table 3. These results indicate that the formation of cracks is related to the shrinkage ratio. The samples with a higher shrinkage ratio exhibited fewer cracks, a lower porosity, and a higher skeleton density.

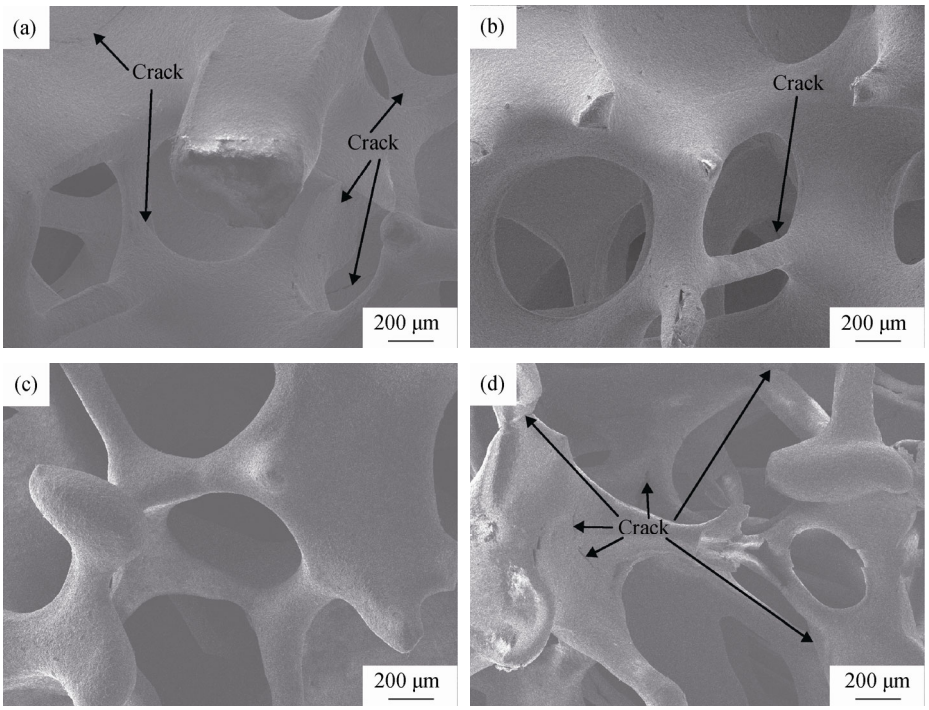

Fig. 8. SEM micrographs of the porous ceramic samples: (a) S1; (b) S2; (c) S3; (d) S4.

Table 3. Porosity, skeleton density, linear shrinkage, and compressive strength of the sintered samples

Samples	Porosity / %		Skeleton density / ($g \cdot cm^{-3}$)		Linear shrinkage / %		Compressive strength / MPa	
	Value	Error	Value	Error	Value	Error	Value	Error
S1	78.7	0.47	2.68	0.039	25.4	0.39	1.33	0.099
S2	77.8	0.43	2.77	0.051	26.6	0.43	1.62	0.087
S3	76.5	0.35	2.87	0.040	28.6	0.41	2.33	0.085
S4	77.5	0.42	2.59	0.052	25.0	0.39	1.21	0.117

The compressive strength, which is one of the main properties of porous materials, is also given in Table 3. The compressive strength was substantially affected by the Al_2O_3 content. Sample S3, whose Al/Si molar ratio was 2.40, exhibited a much higher compressive strength than sample S4, whose molar ratio was 3.00. The compressive strength increased as the mole ratio of Al/Si in the samples was increased from 0.84 to 2.40, but then decreased as the Al_2O_3 content was increased further. The reaction products were the main factors influencing the compressive strength of the porous ceramics. During the sintering process, a moderate SiO_2 amorphous liquid phase is needed to bond all the banded structures together. However, excessive SiO_2 amorphous liquid phase is also detrimental to the quality of the ceramics because the low mechanical quality of the amorphous phase can result in materials with a low compressive strength and cause skeleton cracks, as shown in Figs. 8(a) and 8(b). Because of its SiO_2 amorphous liquid phase binder deficiency and small banded structures, sample S4 contained more cracks than sample S1 or S2. Compared to the other samples, S3 contained an ideal amount of Al_2O_3, which resulted in the S3 porous ceramics exhibiting the highest linear shrinkage, the highest skeleton density, the lowest porosity, and, thus, the highest compressive strength among the investigated porous ceramics.

4. Conclusions

Using coal fly ash samples with different amounts of added Al_2O_3, we prepared porous ceramics by a dipping-polymer-replica approach. The phase compositions, microstructure, and properties of the porous ceramic samples were investigated.

(1) Mullite was the main phase in all of the sintered materials. With increasing Al_2O_3 content, the amount of mullite increased and trace hematite and corundum were detected in the sintered samples.

(2) In the microstructure of sintered samples without added Al_2O_3, crossed banded structures formed and were surrounded by a large amount of amorphous phase. With in-

creasing Al_2O_3 content, the amount of the amorphous phase decreased and the size of the banded structures decreased.

(3) The compressive strength of the porous ceramics was influenced dramatically by the content of Al_2O_3. The compressive strength increased as the Al/Si mole ratio in the samples was increased from 0.84 to 2.40 but then decreased with a further increase in Al_2O_3 content. When coal fly ash was used as a starting material, the mullite-based porous ceramic with an Al/Si mole ratio of 2.40 had a much higher compressive strength and exhibited greater shrinkage than the other samples.

Acknowledgements

This study was financially supported by the Project of the Science and Technology Creative Team of Universities in Jiangxi Province, China (No. 00008713) and by the Open Foundation of Jiangxi Key Laboratory for Advanced Copper and Tungsten Materials (No. 2013-KLP-04).

References

[1] X.G. Deng, J.K. Wang, J.H. Liu, H.J. Zhang, F.L. Li, H.J. Duan, L.L Lu, Z. Huang, W.G. Zhao, and S.W. Zhang, Preparation and characterization of porous mullite ceramics via foam-gelcasting, *Ceram. Int.*, 41(2015), No. 7, p. 9009.

[2] M.H. Talou and M.A. Camerucci, Processing of porous mullite ceramics using novel routes by starch consolidation casting, *J. Eur. Ceram. Soc.*, 35(2015), No. 3, p. 1021.

[3] M.L. Chen, L. Zhu, Y.C. Dong, L.L. Li, and J. Liu, Waste-to-resource strategy to fabricate highly porous whisker-structured mullite ceramic membrane for simulated oil-in-water emulsion wastewater treatment, *ACS Sustain. Chem. Eng.*, 4(2016), No. 4, p. 2098.

[4] G.L. Chen, H. Qi, W.H. Xing, and N.P. Xu, Direct preparation of macroporous mullite supports for membranes by *in situ* reaction sintering, *J. Membr. Sci.*, 318(2008), No. 1-2, p. 38.

[5] Y.C. Dong, S. Hampshire, J.E. Zhou, B. Lin, Z.L. Ji, X.Z. Zhang, and G.Y. Meng, Recycling of fly ash for preparing porous mullite membrane supports with titania addition, *J. Hazard. Mater.*, 180(2010), No. 1-3, p. 173.

[6] J.J. Cao, X.F. Dong, L.L. Li, Y.C. Dong, and S. Hampshire, Recycling of waste fly ash for production of porous mullite ceramic membrane supports with increased porosity, *J. Eur. Ceram. Soc.*, 34(2014), No. 13, p. 3181.

[7] L. Zhu, Y.C. Dong, S. Hampshire, S. Cerneaux, and L. Winnubst, Waste-to-resource preparation of a porous ceramic membrane support featuring elongated mullite whiskers with enhanced porosity and permeance, *J. Eur. Ceram. Soc.*, 35(2015), No. 2, p. 711.

[8] L. Zhu, Y.C. Dong, L.L. Li, J. Liu, and S.J. You, Coal fly ash industrial waste recycling for fabrication of mullite-whisker-structured porous ceramic membrane supports, *RSC Adv.*, 5(2015), No. 15, p. 11163.

[9] H.R. Qian, Y.H. Wang, X.D. Cheng, H.P. Zhang, and R.F. Zhang, Preparation of porous mullite ceramics using fly ash cenosphere as a pore-forming agent by gelcasting process, *Int. J. Appl. Ceram. Technol.*, 11(2014), No. 5, p. 858.

[10] H.S. Guo, W.F. Li, and F.B. Ye, Low-cost porous mullite ceramic membrane supports fabricated from kyanite by casting and reaction sintering, *Ceram. Int.*, 42(2016), No. 4, p. 4819.

[11] J.H. Li, H.W. Ma, and W.H. Huang, Effect of V_2O_5 on the properties of mullite ceramics synthesized from high-aluminum fly ash and bauxite, *J. Hazard. Mater.*, 166(2009), No. 2-3, p. 1535.

[12] Q.K. Lü, X.F. Dong, Z.W. Zhu, and Y.C. Dong, Environment-oriented low-cost porous mullite ceramic membrane supports fabricated from coal gangue and bauxite, *J. Hazard. Mater.*, 273(2014), No. 6, p. 136.

[13] Z.P. Hou, B.X. Cui, L.L. Liu, and Q. Liu, Effect of the different additives on the fabrication of porous kaolin–based mullite ceramics, *Ceram. Int.*, 42(2016), No. 15, p. 17254.

[14] Y.C. Dong, J. Diwu, X.F. Feng, X.Y. Feng, X.Q. Liu, and G.Y. Meng, Phase evolution and sintering characteristics of porous mullite ceramics produced from the flyash–$Al(OH)_3$ coating powders, *J. Alloys Compd.*, 460(2008), No. 1-2, p. 651.

[15] T.Y. Yang, H.B. Ji, S.Y. Yoon, B.K. Kim, and H.C. Park, Porous mullite composite with controlled pore structure processed using a freeze casting of TBA-based coal fly ash slurries, *Resour. Conserv. Recycl.*, 54(2010), No. 11, p. 816.

[16] J.H. Lee, H.J. Choi, S.Y. Yoon, B.K. Kim, and H. C. Park, Porous mullite ceramics derived from coal fly ash using a freeze-gel casting/polymer sponge technique, *J. Porous Mater.*, 20(2013), No. 1, p. 219.

[17] S.H. Li, H.Y. Du, A.R. Guo, and D. Yang, Preparation of self-reinforcement of porous mullite ceramics through *in situ* synthesis of mullite whisker in fly ash body, *Ceram. Int.*, 38(2012), No. 2, p. 1027.

[18] R.S. Blissett and N.A. Rowson, A review of the multi-component utilisation of coal fly ash, *Fuel*, 97(2012), p. 1.

[19] S. Akpinar, I.M. Kusoglu, O. Ertugrul, and K. Onel, *In situ* mullite foam fabrication using microwave energy, *J. Eur. Ceram. Soc.*, 32(2012), No. 4, p. 843.

[20] Y.C. Dong, X.Y. Feng, X.F. Feng, Y.W. Ding, X.Q. Liu, and G.Y. Meng, Preparation of low-cost mullite ceramics from natural bauxite and industrial waste fly ash, *J. Alloys Compd.*, 460(2008), No. 1-2, p. 599.

[21] L.L. Li, X.F. Dong, Y.C. Dong, Y.M. Zheng, L. Zhu, and J. Liu, Thermal conversion of hazardous metal copper via the preparation of $CuAl_2O_4$ spinel-based ceramic membrane for potential stabilization of simulated copper-rich waste, *ACS Sustain. Chem. Eng.*, 3(2015), No. 11, p. 2611.

[22] L.L. Li, X.F Dong, Y.C. Dong, L. Zhu, S.J. You, and Y.F Wang, Incorporation of zinc for fabrication of low-cost spinel-based composite ceramic membrane support to achieve its stabilization, *J. Hazard. Mater.*, 287(2015), p. 188.

[23] J. Liu, Y.C. Dong, X.F. Dong, S. Hampshire, L. Zhu, Z.W. Zhu, and L.L. Li, Feasible recycling of industrial waste coal fly ash for preparation of anorthite-cordierite based porous ceramic membrane supports with addition of dolomite, *J. Eur. Ceram. Soc.*, 36(2016), No. 4, p. 1059.

[24] P. Sarin, W. Yoon, R.P. Haggerty, C. Chiritescu, N.C. Bhorkar, and W.M. Kriven, Effect of transition-metal-ion doping on high temperature thermal expansion of 3:2 mullite: an *in situ*, high temperature, synchrotron diffraction study, *J. Eur. Ceram. Soc.*, 28(2008), No. 2, p. 353.